

Journal of
Applied Remote Sensing

**10.35 μm : atmospheric window on the
GOES-R Advanced Baseline Imager
with less moisture attenuation**

Daniel T. Lindsey
Timothy J. Schmit
Wayne M. MacKenzie, Jr.
Christopher P. Jewett
Mat M. Gunshor
Louie Grasso



10.35 μm : atmospheric window on the GOES-R Advanced Baseline Imager with less moisture attenuation

Daniel T. Lindsey,^a Timothy J. Schmit,^b Wayne M. MacKenzie Jr.,^c
Christopher P. Jewett,^d Mat M. Gunshor,^e and Louie Grasso^f

^aNOAA/NESDIS/STAR/RAMMB, CIRA/CSU, 1375 Campus Delivery, Fort Collins,
Colorado 80523

Dan.Lindsey@noaa.gov

^bNOAA/NESDIS/STAR/ASPB, Madison, Wisconsin

^cEarth Resources Technology, Inc., Laurel, Maryland

^dUniversity of Alabama-Huntsville, Huntsville, Alabama

^eCooperative Institute for Meteorological Satellite Studies, Madison, Wisconsin

^fCooperative Institute for Research in the Atmosphere, Fort Collins, Colorado

Abstract. With the launch of GOES-R expected in 2015, research is currently under way to fully understand the characteristics of every channel on its Advanced Baseline Imager (ABI). The ABI will have two infrared (IR) window bands centered near 10.35 and 11.2 μm . Since no broad-band space-borne sensor has a channel near 10.35 μm , radiative transfer model simulations are used to study the clear-sky gaseous absorption properties in this wavelength range. It is shown that water vapor preferentially absorbs radiation at 11.2 μm compared to 10.35 μm , making the 10.35 μm a “cleaner” window IR band. © 2012 Society of Photo-Optical Instrumentation Engineers (SPIE). [DOI: [10.1117/1.JRS.6.063598](https://doi.org/10.1117/1.JRS.6.063598)]

Keywords: GOES-R; Advanced Baseline Imager; satellite; infrared window; absorption; transmission; water vapor attenuation.

Paper 12171 received Jun. 6, 2012; revised manuscript received Sep. 26, 2012; accepted for publication Oct. 4, 2012; published online Oct. 30, 2012.

1 Introduction

Currently scheduled for launch in late 2015, GOES-R will become the first in a series of satellites for the National Oceanic and Atmospheric Administration (NOAA) carrying a new state-of-the-art imaging payload. Among the new instruments aboard is the Advanced Baseline Imager (ABI),¹ offering significant spatial, temporal, and spectral improvements over the current GOES imager. Work is currently under way to develop new and improved capabilities for the ABI, so that when the satellite is launched, the new data and products will immediately begin flowing to users.²

A list of the bands available on the ABI is provided in Table 1. Note that there are two bands within the traditional infrared (IR) window portion of the spectrum (10 to 12 μm): one centered near 10.35 μm (band 13) and another near 11.2 μm (band 14). Band 15, centered near 12.3 μm , is within the “dirty window,” a term referring to water vapor absorption lines that become more numerous from 10 to 13 μm (Fig. 1). Currently, the expected central wavelength of band 13 for the first ABI is actually 10.33 μm . Schmit et al.¹ state that the 10.35 μm band is “less sensitive to low-level moisture and, hence, helps with atmospheric moisture corrections, cloud particle size, and surface properties.” However, a detailed quantitative analysis of its absorption characteristics has not been published.

The term “window” refers to a band with relatively little atmospheric absorption by gases such as water vapor and carbon dioxide. Window IR channels are normally used for viewing both surface and cloud features, and their brightness temperatures are often used as a proxy for the radiating temperatures of these features, since emissivity values in this wavelength range are

Table 1 Summary of the ABI wavelengths, based on the prototype flight model. Full width at half maximum (FWHM) minimum and maximum values are also listed.

Band	Approximate central wavelength (μm)	FWHM at 50% minimum (μm)	FWHM at 50% maximum (μm)
1	0.47	0.45	0.49
2	0.64	0.60	0.68
3	0.86	0.85	0.88
4	1.38	1.37	1.39
5	1.61	1.59	1.63
6	2.25	2.23	2.27
7	3.90	3.80	4.01
8	6.16	5.78	6.59
9	6.93	6.72	7.14
10	7.34	7.25	7.44
11	8.50	8.31	8.70
12	9.61	9.43	9.81
13	10.33	10.17	10.48
14	11.2	10.8	11.6
15	12.3	11.9	12.8
16	13.3	13.0	13.6

typically 0.96 to 1.0 (Ref. 3). Bands near 11.2 μm can be found on a variety of imagers, including GOES-8 to -15 (10.7 μm), Meteosat Second Generation/Spinning Enhanced Visible and Infrared Imager (10.8 μm), Moderate Resolution Imaging Spectroradiometer (11.0 μm), Visible Infrared Imager Radiometer Suite (10.8 and 11.4 μm), MTSat 2r (10.8 μm), and MeteoSat-7 (11.5 μm). The globe is (and has been) observed in the IR window for decades and such data are heavily utilized for a variety of operational tasks and algorithms. However, no broad-band space-borne instrument has a band centered near 10.3 μm , meaning research is necessary to fully understand the relative advantages of the two ABI window bands. The MODIS Airborne Simulator (MAS)⁴ was flown aboard aircraft in the early 1990s and had a channel centered at 10.55 μm , but this band was ultimately not chosen for the MODIS instrument. This MAS band was used as heritage to the band selected on the ABI. Another option is to simulate the broad bands using high-spectral resolution instruments, such as infrared atmospheric sounding interferometer (IASI)⁵ or cross-track infrared sounder (CrIS). The ABI data will be remapped to a fixed projection. At the satellite sub-point, the pixel spacing will be 1 km for ABI bands 1, 3, and 5, and ABI band 2 will be at 0.5 km. All other ABI spectral bands will be at 2 km.

The goals of this paper are to address two primary questions: (1) What are the relative advantages of the 10.35 and 11.2 μm channels in clear sky conditions? (2) Should one of them be the default atmospheric window IR band on the ABI? To help answer these questions, we will make use of three different radiative transfer models (RTM). Section 2 will present the RTM results and Sec. 3 will summarize the findings.

2 Radiative Transfer Model Simulations

Results from three different RTMs will be presented to avoid any model-specific biases. The goal is to investigate which gases contribute to the absorption characteristics within the 10.35 and 11.2 μm bands.

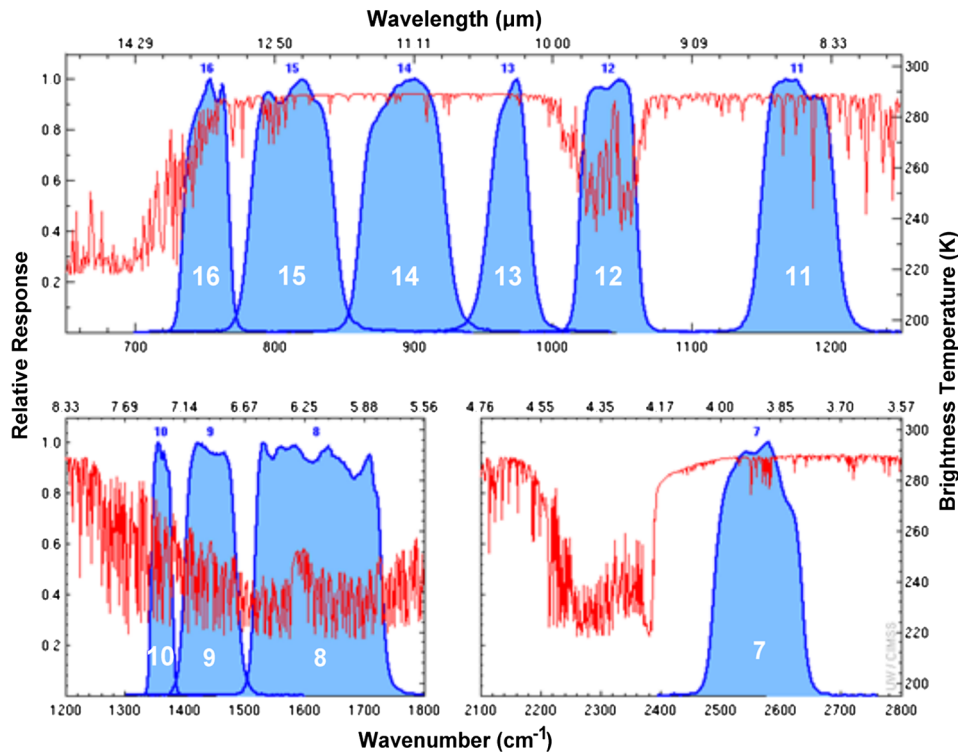


Fig. 1 Spectral response functions (SRF) for the ABI IR bands (blue curves with band numbers indicated in white) along with the calculated absorption lines (red) from the PFAAST model (see Sec. 2.1 below) using the standard U.S. Atmosphere.

2.1 Pressure Layer Fast Algorithm for Atmospheric Transmittances Model

Figure 2 shows a simulation using the Pressure Layer Fast Algorithm for Atmospheric Transmittances Model (PFAAST) RTM,⁶ including the spectral response functions (SRF) for the ABI 10.35 μm , 11.2 μm , and GOES-13 10.7 μm bands. The 10.35 μm SRF is spectrally narrower than both the 10.7 and 11.2 μm SRF and includes no information from any absorption lines greater

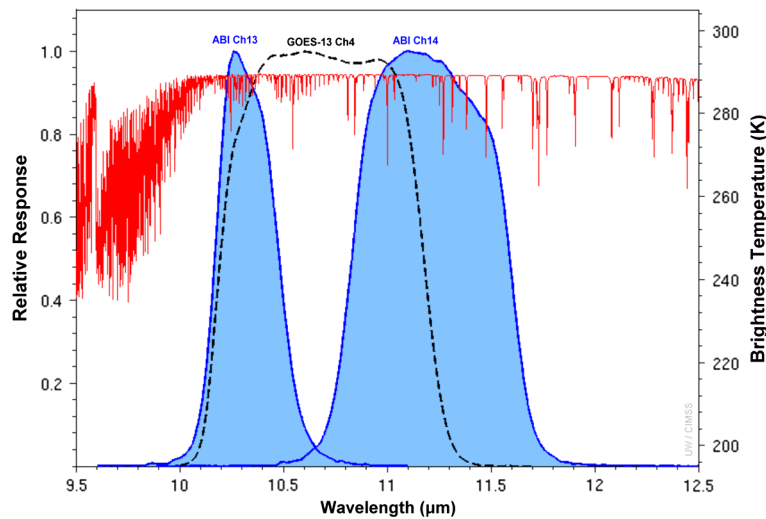


Fig. 2 Spectral response functions (SRF) for the ABI band 13 (10.35 μm , blue curve on the left) and band 14 (11.2 μm , blue curve on the right), along with the GOES-13 Imager band 4 (10.7 μm , black dotted line), and the calculated absorption lines (red) from the PFAAST model using the standard U.S. Atmosphere.

than around 11.0 μm . Note also that the left tail of the 10.35 μm SRF is just less than 10.0 μm , where ozone absorption begins to become significant. The 11.20 μm SRF extends above 11.6 μm and therefore includes some water vapor absorption lines that are common in the region between 11.0 and 12.5 μm . A more detailed examination of the relative contributions of each absorbing gas is found in the next subsection.

2.2 Line-by-Line RTM

In the next series of experiments, the line-by-line RTM (LBLRTM) described in Clough et al.⁷ is used to understand what gases contribute to the brightness temperatures observed at both ABI IR window bands. The LBLRTM heritage is based on FASCOD⁷⁻⁹ and uses the HITRAN database¹⁰ to determine the spectral properties of the various atmospheric constituents. This model allows for high spectral resolution when performing the line calculations. For this study, a spectral resolution of 0.1 cm^{-1} was used to improve the accuracies of the brightness temperature calculations. Surface emissivity values are set to 1.0 for each of these noise-free simulations. Figure 3 shows the sounding used in the simulations in this section. It is a mid-summer morning sounding from Birmingham, Alabama, with a surface temperature of 291.15 K, so although the low-level (surface to 850 hPa) water vapor content is relatively large, the low-level temperature lapse rate is fairly stable. This is important because the effect of water vapor absorption on satellite-observed brightness temperatures is accentuated with unstable lapse rates¹¹ so although the effect of water vapor will be evident in the RTM simulation results, the magnitude would be significantly larger if an afternoon sounding had been used (see Fig. 4 and the associated discussion below).

Simulation results are presented in Figs. 5 to 6. When all absorbing species are included (Fig. 5), the 10.35 μm brightness temperature is approximately 1 K warmer than at 11.2 μm , suggesting more gaseous absorption at 11.2 μm . When all gases besides water vapor are removed (Fig. 7), the spectrum of absorption appears largely the same above about 10.8 μm . Comparing

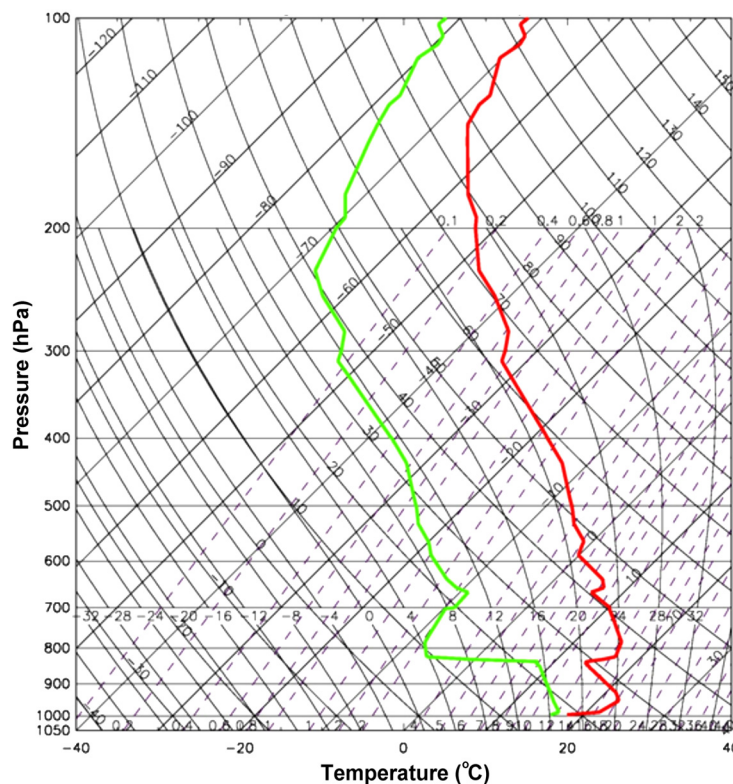


Fig. 3 Sounding from Birmingham, Alabama, at 1200 coordinated universal time (UTC) on 15 July 2008 plotted on a skew-T/log-P. Red is the temperature profile and green is the dew point profile. This sounding was used in all of the experiments using the LBLRTM.

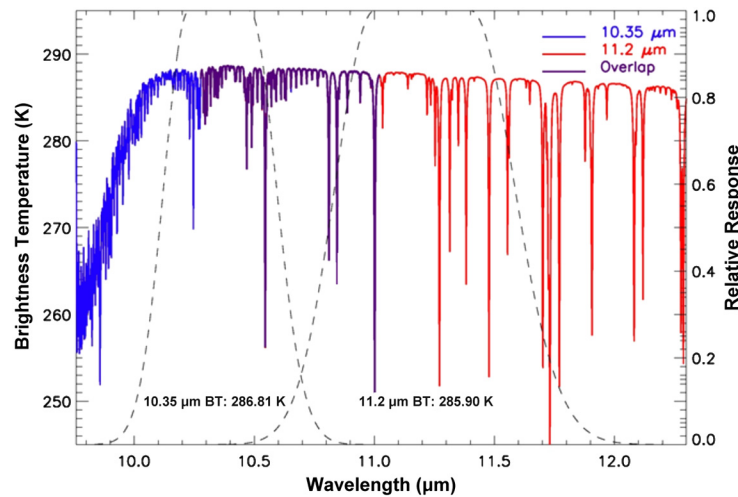


Fig. 4 (a) Simulated 10.35 minus 11.2 μm brightness temperatures (colors, in $^{\circ}\text{C}$) and surface dewpoints (contours, in $^{\circ}\text{C}$) based on a 19 h forecast of the NSSL WRF-ARW from 00 coordinated universal time (UTC) on 29 May 2012, and (b) locations of the model grid columns containing any cloud material at the same time as (a).

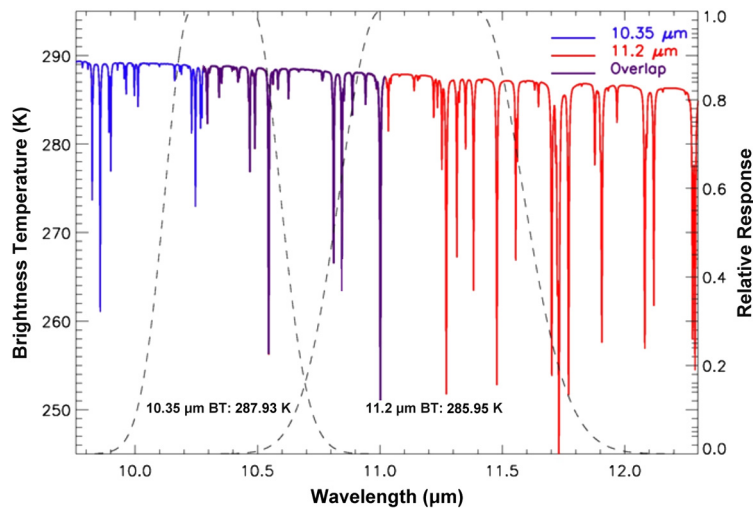


Fig. 5 Results of the LBLRTM using the sounding from Fig. 3. The dashed lines are indicative of the 10.35 and 11.2 μm SRFs. The blue line represents the line-by-line brightness temperatures (K) at 10.35 μm , the red line at 11.2 μm , and the purple line in the region overlapped by both 10.35 and 11.2 μm . The estimated band-integrated satellite-observed brightness temperatures are also indicated for each band. This simulation includes absorption by all species.

the integrated brightness temperatures at 11.2 μm using all species (285.90 K) with that using only water vapor (285.95 K), it is evident that water vapor is responsible for essentially all gaseous absorption within this band; other gases are responsible for only 0.05 K additional cooling in this simulation. At 10.35 μm , however, gases besides water vapor are responsible for 1.13 K cooling, a more significant value.

The two other major atmospheric constituents that absorb longwave radiation within 10.35 μm channel are ozone and carbon dioxide. For Figs. 6 and 8, profiles of ozone and carbon dioxide were set to the 1976 U.S. Standard Atmosphere values. Figure 8 shows the results when only ozone is included. The ozone absorption region around 9.5 μm extends to around 10.0 μm , so as was mentioned above, the 10.35 μm band experiences a small amount of ozone absorption. Comparing the two brightness temperatures, ozone is responsible for about 0.5 K cooling relative to the 11.20 μm band, which has no absorption at all in this simulation. Carbon dioxide also

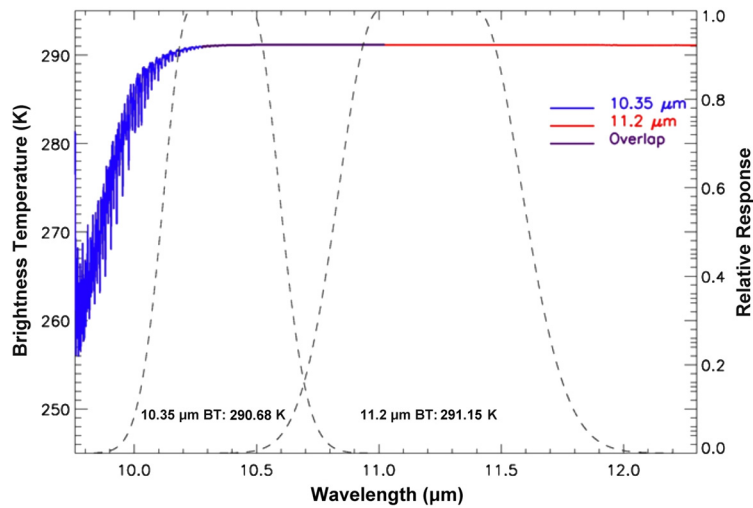


Fig. 6 Same as Fig. 5, except with only carbon dioxide absorption included.

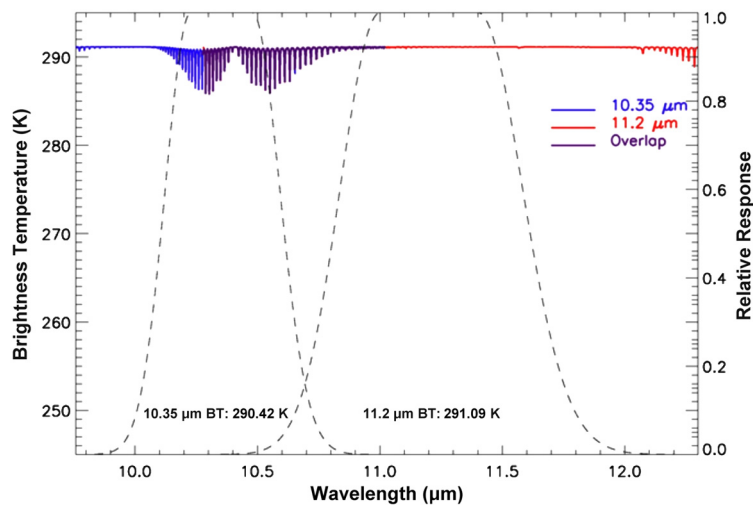


Fig. 7 Same as Fig. 5, except with only water vapor absorption included.

has some small absorption lines between 10.0 and 11.0 μm (Fig. 6) which produce about 0.7 K cooling in the 10.35 μm band in this simulation, while the 11.20 μm remains almost completely unaffected. The combined cooling from ozone and carbon dioxide is about 1.2 K in the 10.35 μm band, and near zero in the 11.2 μm .

In summary, water vapor absorption is more significant in the 11.2 μm band compared to the 10.35 μm band, and the magnitude of the cooling associated with water vapor depends strongly on the temperature and water vapor profiles. A closer examination of water vapor absorption appears in the following subsection. Slight cooling associated with ozone and carbon dioxide occurs at 10.35 μm , but given that these gases are relatively horizontally homogeneous, the magnitude of cooling is easily predicted and thus accounted for in satellite radiance measurements.

2.3 Optical Path Transmittance

A third RTM run at the Cooperative Institute for Research in the Atmosphere (CIRA) makes use of Optical Path Transmittance (OPTRAN)¹² to calculate gaseous absorption. The three gas types are water vapor, ozone, and “dry gases,” which refer to all gases besides water vapor and ozone. In these experiments, the goal is to quantify the cooling associated with water vapor absorption at the 10.35 and 11.2 μm bands. Figure 9 shows the 10 soundings used in the sensitivity tests, or an

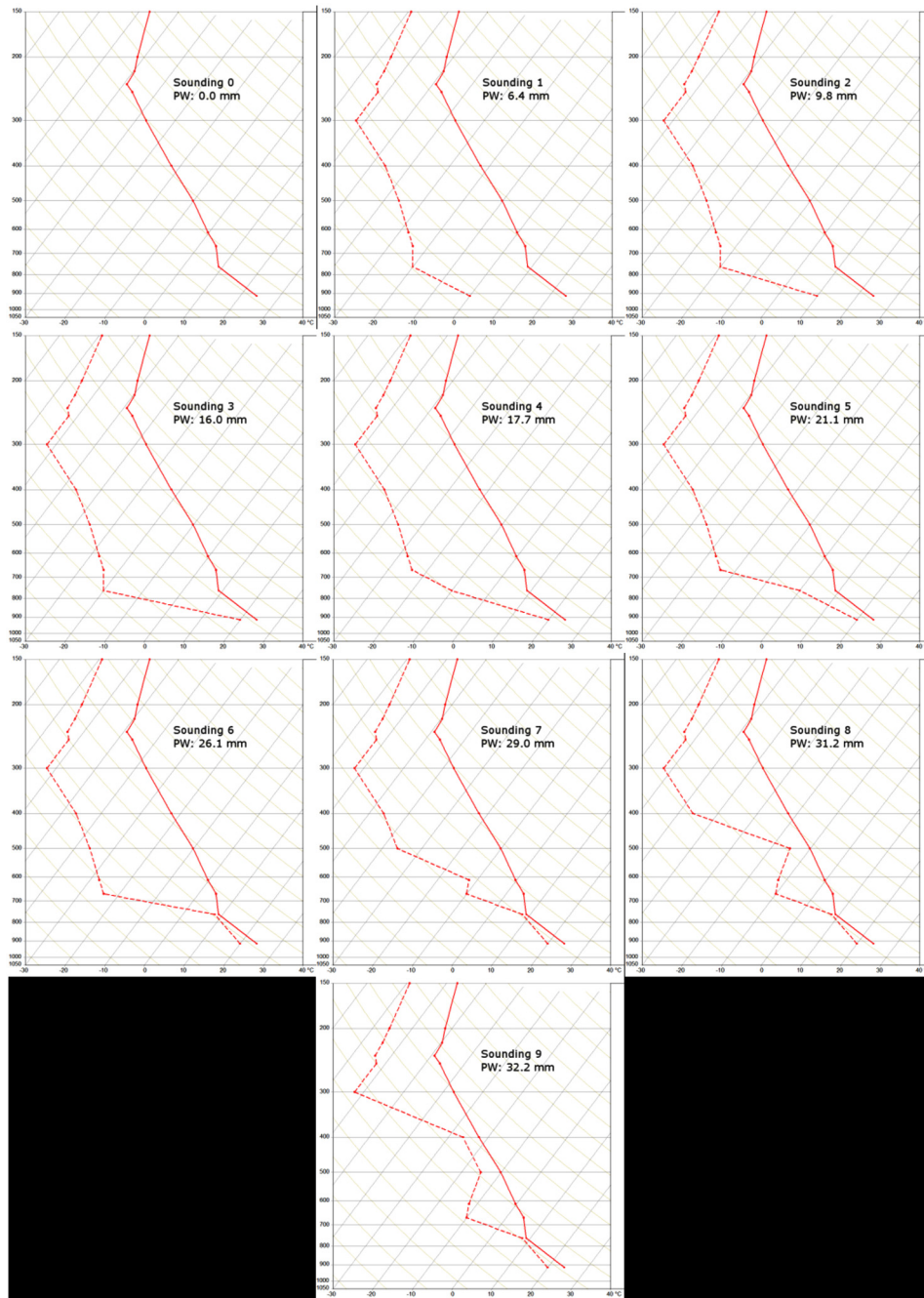


Fig. 8 Same as Fig. 5, except with only ozone absorption included.

animation (Video 1) can be viewed to see larger versions of all 10 soundings. Each sounding has a surface temperature of 297.35 K and identical temperature profiles in the vertical, but the dew point profiles exhibit increasing total precipitable water. Sounding 0 has zero water vapor in the column. For simplicity, surface emissivity values are set to 1.0 for both bands.

For the initial set of simulations, all absorbing species besides water vapor are removed; the results are shown in Fig. 10. For sounding 0 (zero water vapor), the 10.35 and 11.2 μm brightness temperatures are the same, verifying that no differential absorption is occurring in the atmosphere (by design). For each additional sounding having increasing total precipitable water, the 11.2 μm brightness temperature decreases more rapidly than the 10.35 μm brightness temperature, and the magnitude of the difference is about 1.3 K for sounding 9. This shows that water vapor indeed preferentially absorbs radiation in the 11.2 μm band compared to the

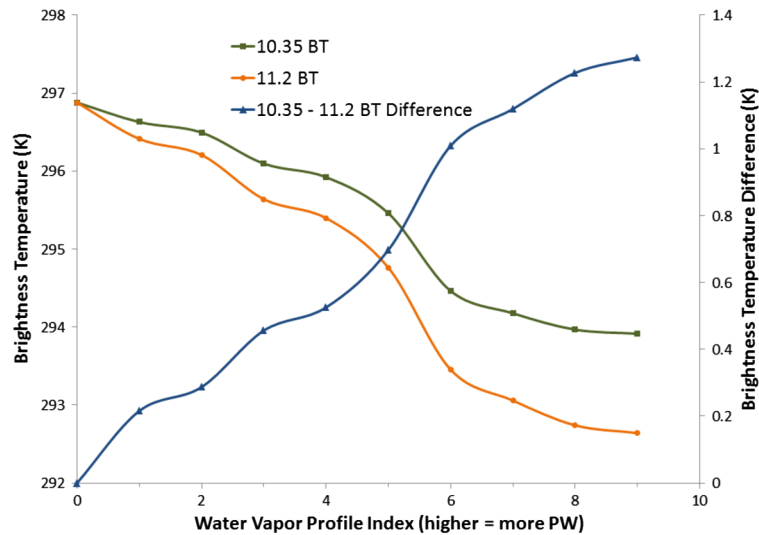


Fig. 9 Ten temperature (solid) and dew point (dashed) soundings used in the OPTRAN sensitivity tests plotted on skew-T/log-P diagrams. An animation (Video 1) can be viewed to see larger versions of all 10 soundings. The total precipitable water is indicated for each one. Sounding 0 contains no water vapor, so a dew point profile was not plotted, then for the remaining soundings (1 to 9) the water vapor increases first in the lower, then middle, then upper troposphere. The temperature profiles are identical in each sounding, and the vertical axis has units of hPa. (MPG, 0.5 MB) [URL: <http://dx.doi.org/10.1117/1.JRS.6.XXXXXX>].

10.35 μm band, and that 10.35 μm is a cleaner channel in terms of water vapor. Referring back to soundings 8 and 9 in the sounding animation (Video 1), note that the only difference is an increase in the dewpoint in the 300 to 500 hPa range. Figure 10 shows that this mid-level increase in moisture causes very small cooling at both 10.35 and 11.2 μm , showing that low-level dewpoint increases have a more significant impact on satellite-observed brightness temperatures than mid- or upper-level moisture changes. Atmospheric transmission is a function of water vapor mixing ratio, and since mixing ratio values are more than an order of magnitude larger in the lower troposphere compared to the upper troposphere, changes in total precipitable water and in 10.35 and 11.2 μm transmission are dominated by low-level water vapor variations.

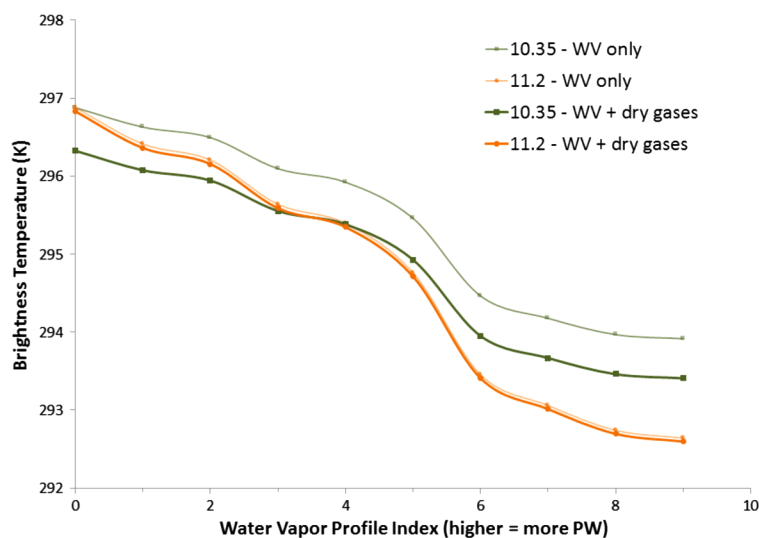


Fig. 10 Simulated brightness temperatures at 10.35 μm (green) and 11.2 μm (orange), and the brightness temperature difference between 10.35 and 11.2 μm (blue) from OPTRAN, using the 9 different input soundings shown in Fig. 7. Water vapor is the only absorbing gas used in these simulations.

Increasing the complexity, Fig. 11 shows the results after allowing dry gas absorption in addition to water vapor. The water vapor-only results are shown again with the light shaded lines for reference. Note that the 10.35 μm brightness temperatures cool about 0.5 μK for all water vapor amounts, while the 11.2 μm brightness temperatures cool only a fraction of 1 K. This effect is consistent with the LBLRTM's cooling due to carbon dioxide absorption. Given the 0.5 μK cooling, the 10.35 μm brightness temperatures are cooler than the 11.2 μm brightness temperatures for soundings 0 to 3, but for the remaining soundings, cooling due to water vapor absorption exceeds 0.5 μK and the 11.2 μm becomes cooler than the 10.35 μm values.

For the final set of experiments, all absorbing species (water vapor, dry gases, and ozone) are included (Fig. 12). Ozone provides no cooling at 11.2 μm because no ozone absorption lines exist within its SRF (Fig. 8), but the 10.35 μm brightness temperature cools an additional 0.2 μK for all water vapor values. The net result of dry gas and ozone absorption is therefore a 0.7 μK cooling at 10.35 μm and only negligible cooling at 11.2 μm .

In order to see how the clear-sky water vapor absorption differences are manifested on a warm season afternoon over the U.S., simulated images were generated at 10.35 and 11.2 μm from output of the 4-km NSSL WRF-ARW. Details on how this processing was executed can be found in Bikos et al.¹³ Figure 4(a) shows the 10.35 to 11.2 μm difference from the 19 h forecast of the 00 coordinated universal time (UTC) run of the NSSL WRF on 29 May 2012. Surface dewpoint values are also plotted for comparison. Positive difference values can be found across east Texas, most of Oklahoma and Kansas, and areas generally east of there. Maximum differences are near +3°C. Negative differences are primarily between 0 and -1 across much of the southwest U.S. Most of the negative values in the eastern half of the domain are associated with clouds [see Fig. 4(b) for the cloud locations], so for simplicity, focus only on the cloud-free regions. Comparing the difference values to the surface dewpoints, the transition from negative to positive in west Texas and near the Colorado/Kansas border roughly corresponds to a surface dryline, i.e., a region with a large horizontal surface dewpoint gradient. These results are consistent with the RTM findings above. Relatively dry regions (such as the desert southwest) have insufficient water vapor to offset the cooling effect of the dry gases, resulting in 11.2 μm brightness temperatures slightly warmer than at 10.35 μm . But in the more moist regions, preferential water vapor absorption at 11.2 μm compared to 10.35 μm results in positive differences as high as +3°C. Surface emissivity values do vary somewhat between 10.35 and 11.2 μm , but the clear-sky brightness temperature difference values shown in Fig. 4(a) are dominated by differences in gaseous absorption.

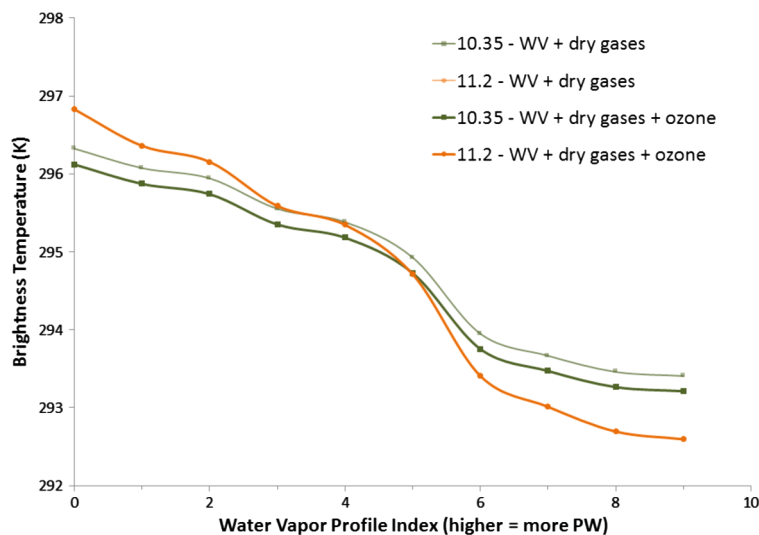


Fig. 11 Similar to Fig. 10, except that dry gas absorption is added. The light green and orange lines show the same data as in Fig. 8 for reference, and the dark green and dark orange lines show the results including both water vapor and dry gas absorption.

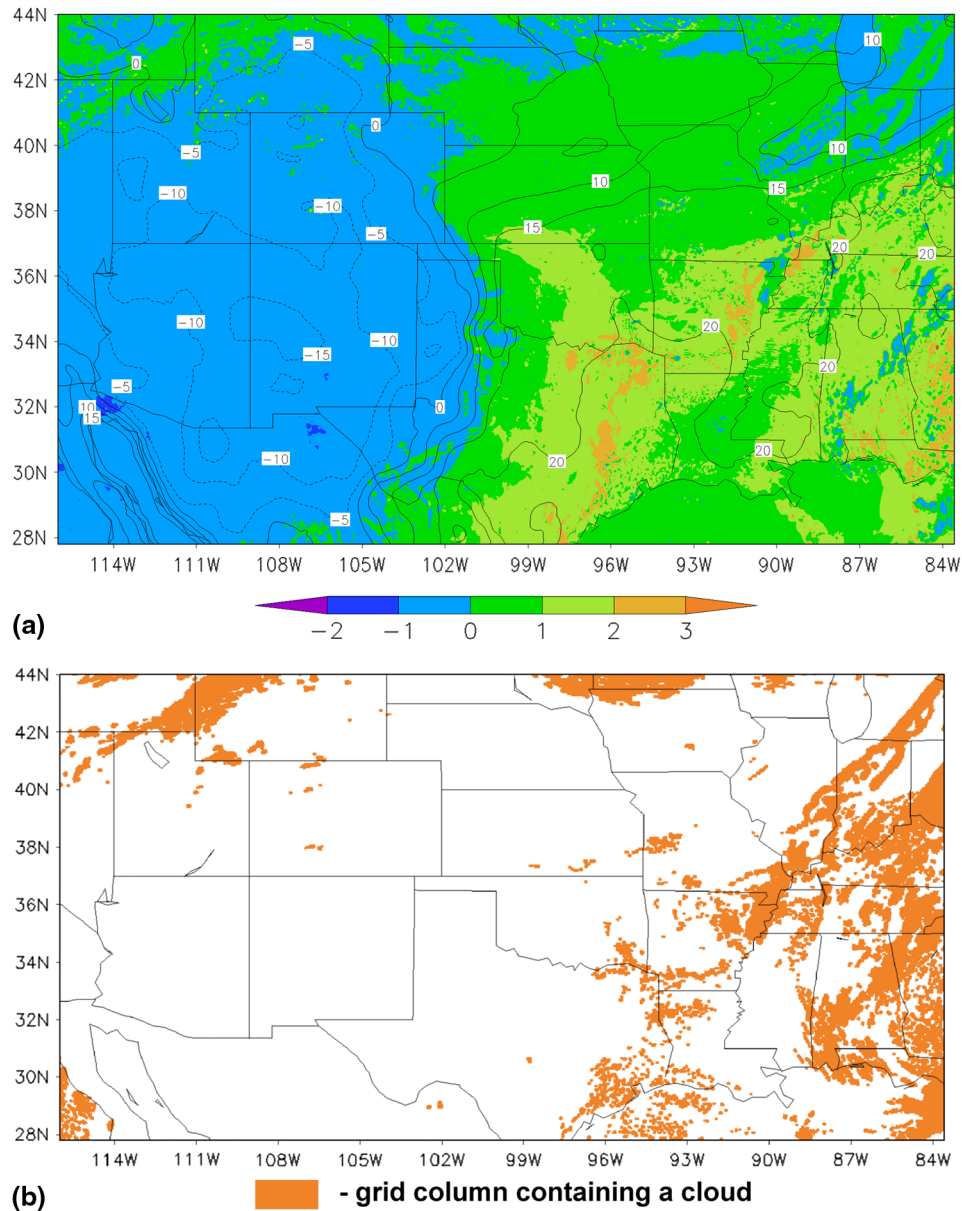


Fig. 12 Similar to Fig. 11, except that the dark green and orange lines show the results including all absorbing species (water vapor, dry gases, and ozone).

3 Summary

The GOES-R ABI will have two window IR bands at 10.35 and 11.2 μm , and given that a channel centered near 10.35 μm has never been aboard a broad-band space-borne imager, research is needed to understand the relative advantages of each band. Two questions were introduced earlier, and are repeated here with answers.

1. What are the relative advantages of the 10.35 and 11.2 μm channels in clear sky conditions?
More outgoing radiation at 11.2 μm is absorbed and re-emitted by water vapor compared to 10.35 μm , making the 10.35 μm a “cleaner” channel with respect to water vapor absorption. There is also a very small amount of ozone and carbon dioxide absorption at 10.35 μm , but the amount of cooling that results is typically less than 1 K and could be corrected for due to the homogeneity of ozone and carbon dioxide. The 11.2 μm channel is useful in many cloud property retrievals due to the cloud particle absorption characteristics in this wavelength range.

2. Should 10.35 or 11.2 μm be the default atmospheric window IR band on the ABI? Since the 10.35 μm band is cleaner than the 11.2 μm band, we recommend that forecasters default to the 10.35 μm band when simply looking at a window IR for estimates of radiating temperatures or subjective cloud identification and classification. But when a more detailed physical retrieval is being designed, characteristics of both bands need to be carefully considered. That said, both bands (in fact all bands from the ABI) are planned to be available for use by forecasters and others.

One clear-sky application of the 10.35 μm band that is currently under investigation involves the 10.35 to 12.3 μm difference, or “split window difference.” A brief discussion of this work can be found in Bikos et al.¹³ Brightness temperature differences between these two bands are due almost exclusively to differential water vapor absorption, so when taking the difference between them, the resulting value is strongly correlated with the amount of total column water vapor. Given that the 10.35 μm band is cleaner than the 11.2 μm band, it makes more sense to use 10.35 μm when forming this split window difference because a stronger water vapor signal will result.

This paper has focused on the relative advantages of the two window IR bands on the ABI with respect to gaseous absorption. An equally important topic is the absorption and scattering characteristics of clouds at these wavelengths. Absorption and scattering by cloud particles are a function of many things, including optical depth, habit, and size distribution. A comprehensive treatment of this topic is beyond the scope of this paper, but we refer readers to the GOES-R Algorithm Theoretical Basis Documents (<http://www.goes-r.gov/products/baseline.html>), in which ABI cloud property retrievals are described in detail.

Acknowledgments

This material is based on work supported by the National Oceanic and Atmospheric Administration under Grant NA090AR4320074. The authors would like to thank Drs. John Knaff and Don Hillger, as well as two anonymous reviewers, for providing insightful comments on this paper. We also thank the GOES-R Project Office. The views, opinions, and findings in this report are those of the authors, and should not be construed as an official NOAA and or U.S. government position, policy, or decision.

References

1. T. J. Schmit et al., “Introducing the next-generation Advanced Baseline Imager (ABI) on GOES-R,” *Bull. Am. Meteor. Soc.* **86**(8), 1079–1096 (1995), <http://dx.doi.org/10.1175/BAMS-86-8-1079>.
2. S. J. Goodman et al., “The GOES-R proving ground: accelerating user readiness for the next-generation geostationary environmental satellite system,” *Bull. Am. Meteor. Soc.* **93**(7), 1029–1040 (2012), <http://dx.doi.org/10.1175/BAMS-D-11-00175.1>.
3. F. Nerry, J. Javed, and M. P. Stoll, “Spectral properties of land surfaces in the thermal infrared: 2. field method for spectrally averaged emissivity measurements,” *J. Geophys. Res. Solid Earth* **95**(B5), 7045–7054 (1990), <http://dx.doi.org/10.1029/JB095iB05p07045>.
4. M. D. King et al., “Airborne scanning spectrometer for remote sensing of cloud, aerosol, water vapor, and surface properties,” *J. Atmos. Ocean. Technol.* **13**, 777–794 (1996), [http://dx.doi.org/10.1175/1520-0426\(1996\)013<0777:ASSFRS>2.0.CO;2](http://dx.doi.org/10.1175/1520-0426(1996)013<0777:ASSFRS>2.0.CO;2).
5. F. Hilton et al., “Hyperspectral earth observation from IASI: five years of accomplishments,” *Bull. Am. Meteor. Soc.* **93**(3), 347–370 (2012), <http://dx.doi.org/10.1175/BAMS-D-11-00027.1>.
6. S. Hannon, L. L. Strow, and W. W. McMillan, “Atmospheric infrared fast transmittance models: a comparison of two approaches,” *Proc. SPIE* **2830**, 94–105 (1996), <http://dx.doi.org/10.1117/12.256106>.
7. S. A. Clough et al., “Atmospheric radiative transfer modeling: a summary of the AER codes, short communication,” *J. Quant. Spectrosc. Radiat. Trans.* **91**(2), 233–244 (2005), <http://dx.doi.org/10.1016/j.jqsrt.2004.05.058>.

8. S. A. Clough, M. J. Iacono, and J.-L. Moncet, "Line-by-line calculation of atmospheric fluxes and cooling rates: application to water vapor," *J. Geophys. Res.* **97**(D14), 15761–15785 (1992), <http://dx.doi.org/10.1029/92JD01419>.
9. S. A. Clough et al., "Atmospheric spectral transmittance and radiance: FASCOD1B," *Proc. SPIE* **277**, 152–166 (1981), <http://dx.doi.org/10.1117/12.931914>.
10. L. S. Rothman et al., "The HITRAN 2008 molecular spectroscopic database," *J. Quant. Spectrosc. Radiat. Trans.* **110**(9–10), 533–572 (2009), <http://dx.doi.org/10.1016/j.jqsrt.2009.02.013>.
11. D. Chesters, L. W. Uccellini, and W. D. Robinson, "Low-level water vapor fields from the VISSR Atmospheric Sounder (VAS) "split window" channels," *J. Appl. Meteor.* **22**(5), 725–743 (1983), [http://dx.doi.org/10.1175/1520-0450\(1983\)022<0725:LLWVFF>2.0.CO;2](http://dx.doi.org/10.1175/1520-0450(1983)022<0725:LLWVFF>2.0.CO;2).
12. L. M. McMillin et al., "Atmospheric transmittance of an absorbing gas, 4: OPTRAN: a computationally fast and accurate transmittance model for absorbing gases with fixed and variable mixing ratios at variable viewing angles," *Appl. Opt.* **34**(27), 6269–6274 (1995), <http://dx.doi.org/10.1364/AO.34.006269>.
13. D. Bikos et al., "Synthetic satellite imagery for real-time high resolution model evaluation," *Weather Forecast.* **27**(3), 784–795 (2012), <http://dx.doi.org/10.1175/WAF-D-11-00130.1>.

Biographies and photographs of the authors are not available.